Supporting Information

Water Oxidation Catalyst via Heterogenization of Iridium Oxides on Silica: A Polyamine-Mediated Route to Achieve Activity and Stability

Nagaraju Shilpa,[†,‡] Joydeb Manna,[†] Parasmani Rajput,[§] and Rohit Kumar Rana[†,‡]*

[†]Nanomaterials Laboratory, I & PC Division, CSIR – Indian Institute of Chemical Technology, Hyderabad 500007, India
[‡]Academy of Scientific and Innovative Research, CSIR – Indian Institute of Chemical Technology, Hyderabad 500007, India
[§]Atomic & Molecular Physics Division, Bhabha Atomic Research Centre, Trombay, Mumbai 400085, India
*To whom correspondence to be addressed email: rkrana@iict.res.in

EXPERIMENTAL SECTION

Materials: Tetraethylorthosilicate (TEOS), N-Cetyl N, N, N- trimethyl ammonium bromide (CTAB), Poly(allylamine hydrochloride) (PAH, 15 KDa), Iridium (IV) oxide, Iridium chloride hydrate ($IrCl_3.xH_2O$) and ceric ammonium nitrate (($NH_4)_2Ce(NO_3)_6$) were procured from Sigma-Aldrich, India. Ammonia solution obtained from S. D fine-chemicals, India. Nitric acid solution was prepared from concentrated nitric acid (Trace Metal Grade, ≥65%, Sigma-Aldrich). All the solutions were prepared using deionized water (18.2 MΩ, Millipore water purification system).

Synthesis of Mesoporous silica: In a typical synthesis of mesoporous silica, 7.24 mL of 0.5 M TEOS in 2 M ammonia solution was mixed with 4.34 mL of 0.1 M CTAB with constant stirring at 300 K for 15 h. The turbid solution was aged for 15 h with constant stirring at room temperature. The resulted silica spheres were collected by centrifugation at a speed of 12000 rpm for 5 min with successive washing with deionized water for four times and then dried at room temperature. Thus obtained material was calcined at 823 K for 5 h with a heating rate of 5° C/min in air in order to remove CTAB.
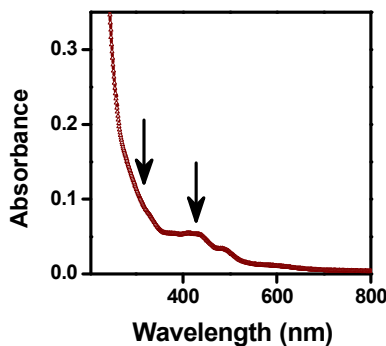

Figure S1: UV-vis spectrum of iridium chloride in an aqueous solution. The iridium precursor in aqueous solution exhibits an absorbance at 310 nm (corresponding to hydroxides of iridium), 420 nm (corresponding to chlorides of iridium) and 480 nm (corresponding to oxidised product of iridium precursor) in solution.[1] Arrows in the spectrum indicate absorbance at 320 nm and at 420 nm .
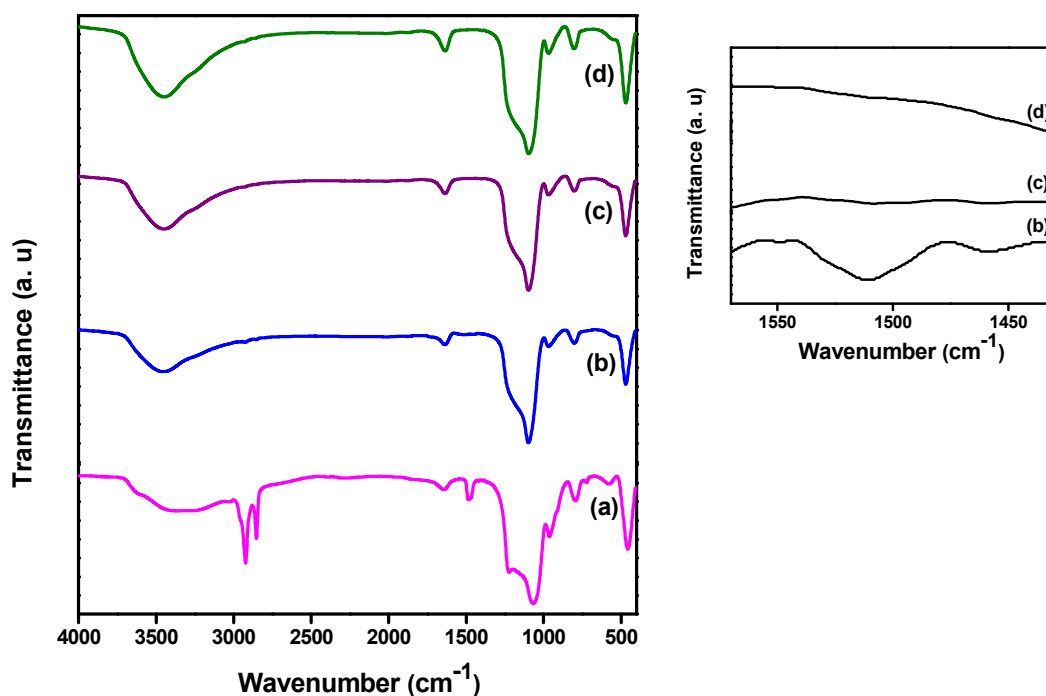
Figure S2: FT-IR spectra for (a) silica spheres, (b) Ir@MS-RT, (c) Ir@MS-MT and (d) Ir@MS-HT and the Inset figure in the right side show the spectra in N-H vibrational region. Absence of the vibrational bands at ca. 2925 cm^{-1} and ca. 2853 cm^{-1} which corresponds to asymmetric and symmetric stretching of methylene groups along with ca. 1484 cm^{-1} corresponding to the N-H bending vibration in the WOCs justifies the removal of CTAB. The typical asymmetric and symmetric stretching modes of the Si-O-Si vibrations at ca. 1097 cm^{-1} and ca. 800 cm^{-1} along with the band at ca. 460 cm^{-1} for Si-O-Si bending modes were observed for the mesoporous silica spheres. Bands at ca. 1643 cm^{-1} and ca. 3382 cm^{-1} corresponds to O-H bending and stretching vibrations of the silanol groups. Iridium oxide normally exhibits Ir-O stretching vibrations at ca. 550 cm^{-1} and ca. 800 cm^{-1} [2]. Vibrational stretching frequency of Ir-O in iridium oxide at ca. 800 cm^{-1} overlaps with Si-O-Si interaction in silica. A band at ca. 963 cm^{-1} for Si-O-metal stretching vibrations whose intensity ratio with ca. 1097 cm^{-1} of Si-O-Si asymmetric stretching was increased upon thermal treatment indicating Si-O-Ir bond formation. The presence of N-H vibrational band at 1480-1540 cm^{-1} in Ir@MS-RT (Inset Figure) depicts the functionalization of silica surface with PAH. The absence of this vibrational band with thermal treatment clearly indicates the decomposition of PAH in Ir@MS-MT and Ir@MS-HT.
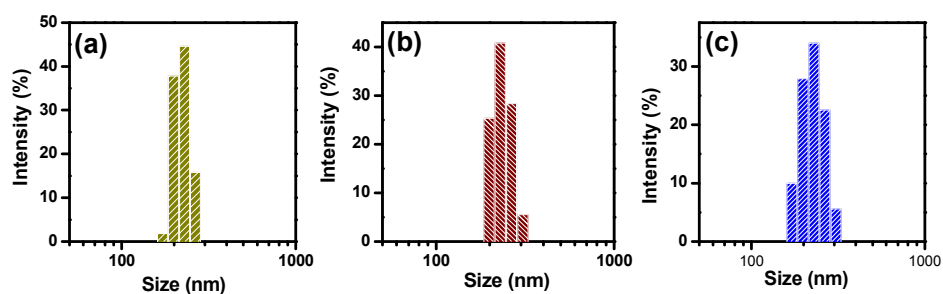
Figure S3: Hydrodynamic particle size of (a) Ir@MS-RT, (b) Ir@MS-MT and (c) Ir@MS-HT respectively as monitored by Dynamic Light Scattering measurement. Hydrodynamic diameter of the particles in Ir@MS-RT and Ir@MS-MT did not change with the average size remaining at ~220 nm similar to that of silica support. A slight increase in diameter was observed for Ir@MS-HT with a size distribution of 160 - 330 nm. There was a reduction in surface charge for the thermally treated samples, plausibly signifying formation of oxides of iridium via condensation of the negatively charged iridium hydroxides.
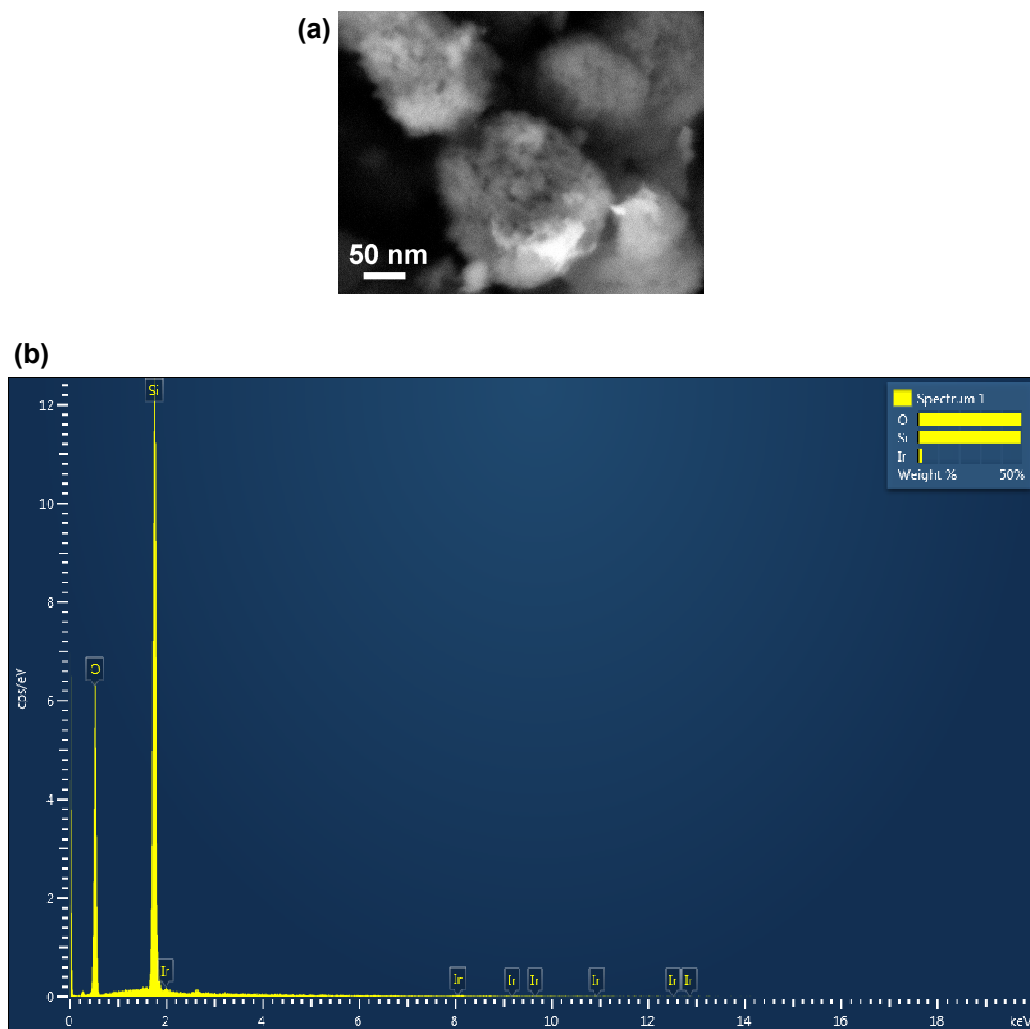
(a)

50 nm

(b)

Figure S4: (a) FE-SEM LABE image of Ir@MS-HT depicting iridium oxide brighter spots on silica surface; (b) EDX spot analysis indicating the presence of Ir, Si and O.
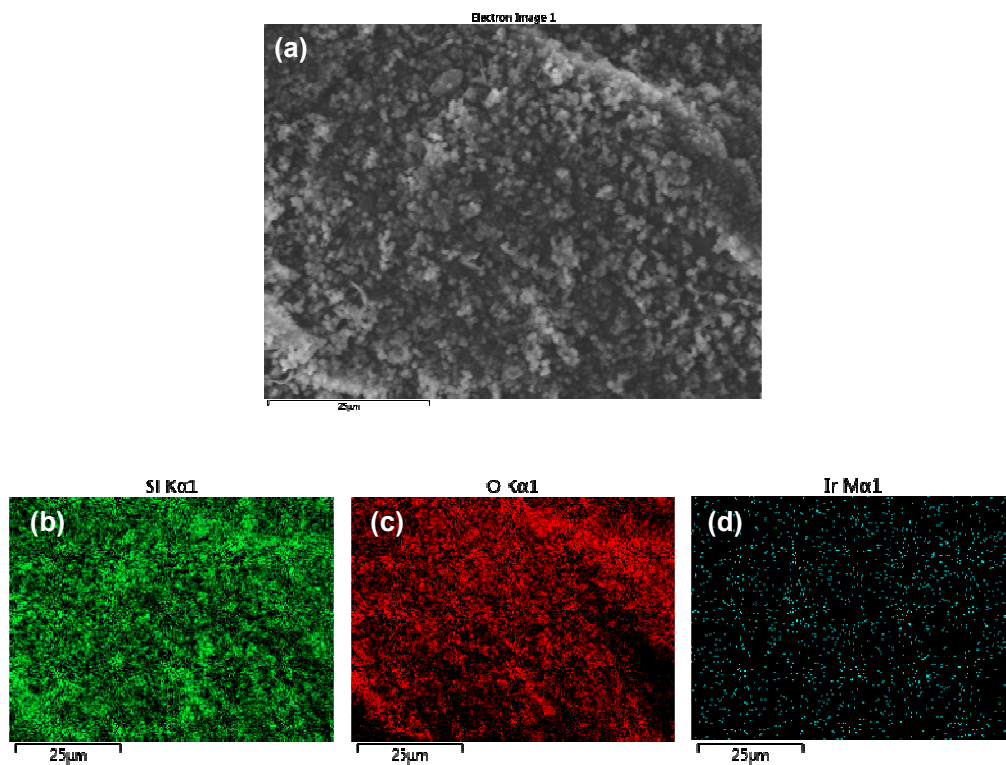
Figure S5: (a) FE-SEM image and (b, c & d) corresponding EDX mapping for the element Si, O, and Ir, respectively for Ir@MS-MT (3.66 Wt% iridium) sample.
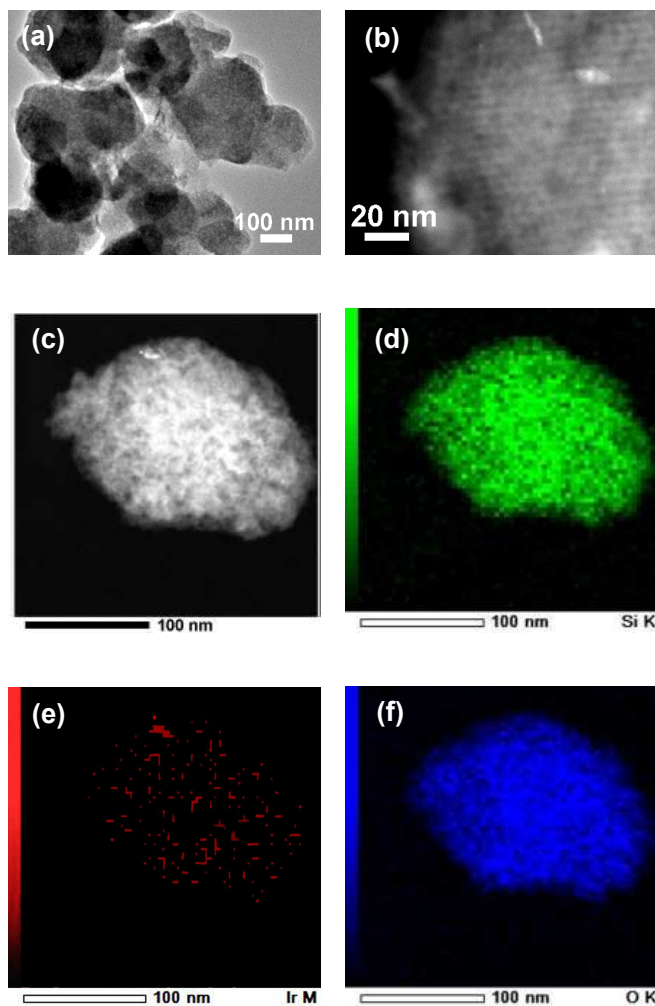
Figure S6: (a & b) STEM-HAADF images of Ir@MS-MT showcasing iridium distribution on mesostructure silica at different magnifications. (c) Bright field image and (d, e & f) corresponding STEM-EDX mapping for the element Si, Ir, and O, respectively for Ir@MS-MT.
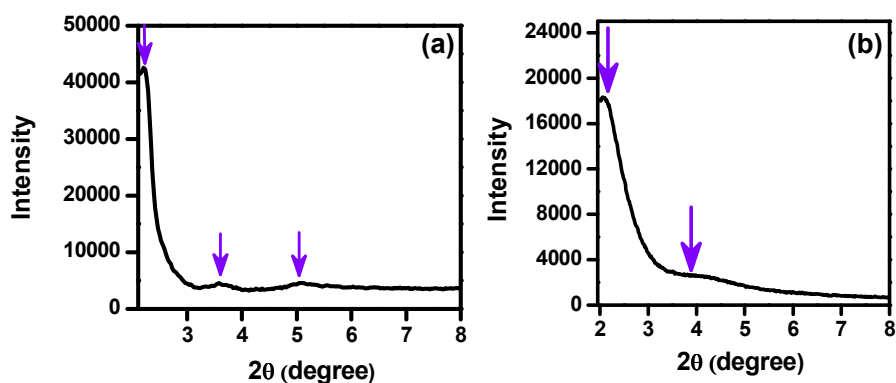
Figure S7: Low angle XRD patterns of (a) MS and (b) Ir@MS-RT. The lattice parameter a_o is calculated from the XRD data using the formula $a_o = (2/\sqrt{3}) d_{100}$, where d_{100}= 4.06 and wall-thickness = a_o – d (d = pore diameter). The lattice parameter a_o was estimated to be 4.68 nm with a wall thickness of 1.85 nm. The intensity of low angle peak decreased upon functionalization as seen for Ir@MS-RT.
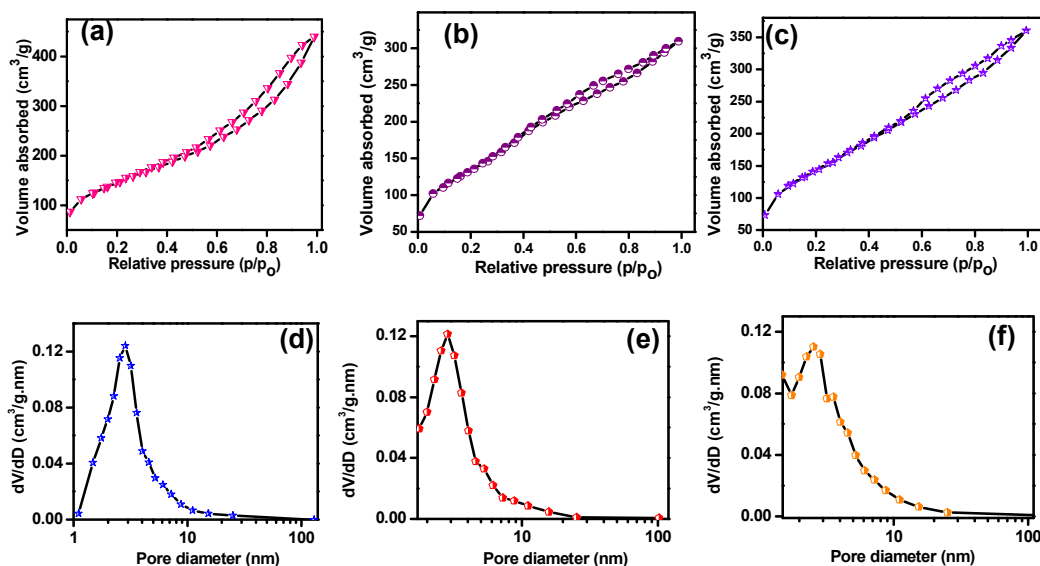

Figure S8: (a, b & c) N_2 adsorption/desorption isotherms and (d, e & f) corresponding BJH pore size distribution plots obtained for Ir@MS-RT, Ir@MS-MT and Ir@MS-HT, respectively. N_2 physisorption analysis showed a decrease in BET surface area and pore volume after functionalization indicating pore-filling by the catalytic species (Table S1). The typical isotherm with a hysteresis loop highlights the mesoporosity in the material. BJH (Barret-Joyner-Halenda) pore-size distribution showed a maximum at 2.8 nm for Ir@MS-RT, which remained similar for Ir@MS-MT as well. Only in case of Ir@MS-HT, there was a decrease in the pore size reflecting growth of the oxides of iridium upon thermal treatment at high temperature (Table S1).
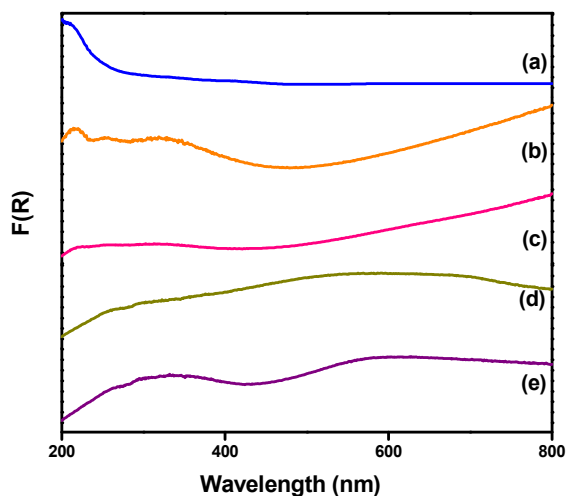
Figure S9: UV-vis Diffuse reflectance spectra of (a) Ir@MS-RT, (b) Ir@MS-MT, (c) Ir@MS-HT, (d) iridium oxide and (e) iridium hydroxide. Iridium hydroxide and iridium oxide were synthesized by following reported method with little modification.[3] $IrCl_3$ solution was adjusted to pH ~ 10 by using 5 M NaOH with continuous stirring at 373 K for a period of 1 h. The obtained precipitate was centrifuged and washed successively with distilled water followed by drying at 338 K for 10 h. Iridium hydroxide obtained was XRD amorphous. Iridium oxide was obtained by thermal treatment of iridium hydroxide at 773 K for a period of 5 h at a heating rate of 2°C/min.
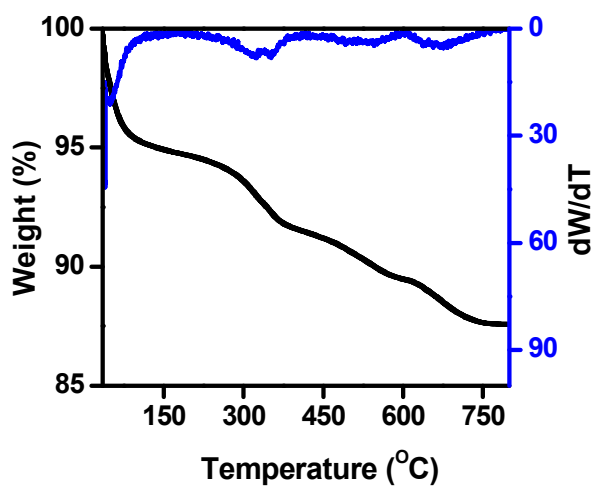

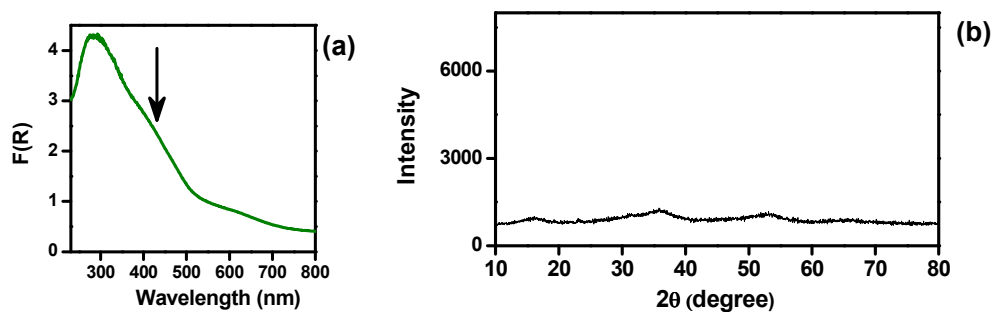Figure S10: TG-DTA profile of Ir@MS-RT obtained under air atmosphere.

Figure S11: (a) UV-vis Diffuse Reflectance spectrum, (b) XRD pattern of thermally treated $IrCl_3$ at 573 K for 5h. The arrow mark in (a) indicates the absorbance at 420 nm due to the presence of chloride containing iridium species.
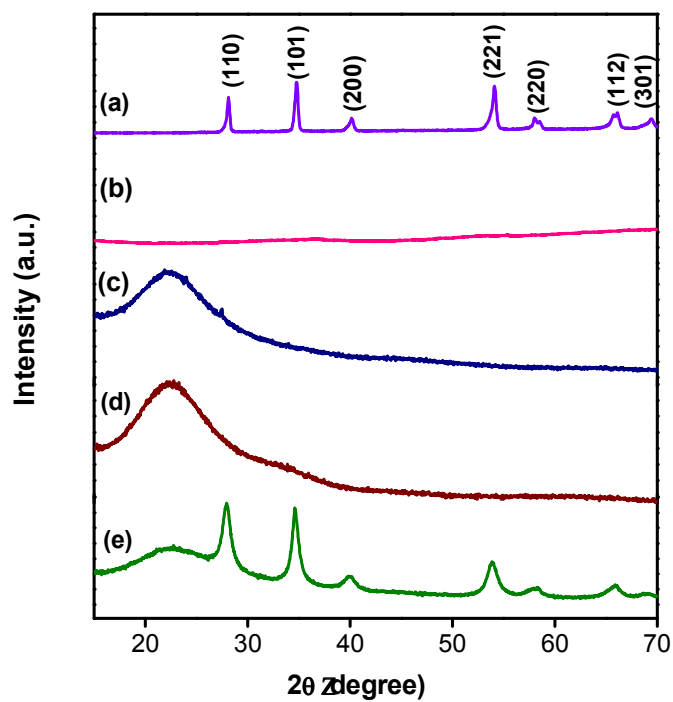

Figure S12: XRD patterns of (a) IrO_2, (b) $IrCl_3$, (c) Ir@MS-RT, (d) Ir@MS-MT, and (e) Ir@MS-HT.
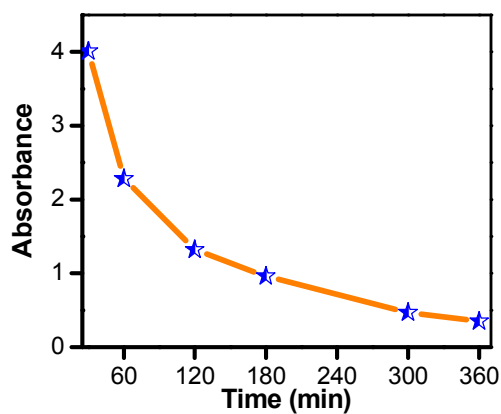
Figure S13: UV-vis absorbance obtained at various time intervals during OER indicating the change in CAN concentration upon reaction with Ir@MS-MT.
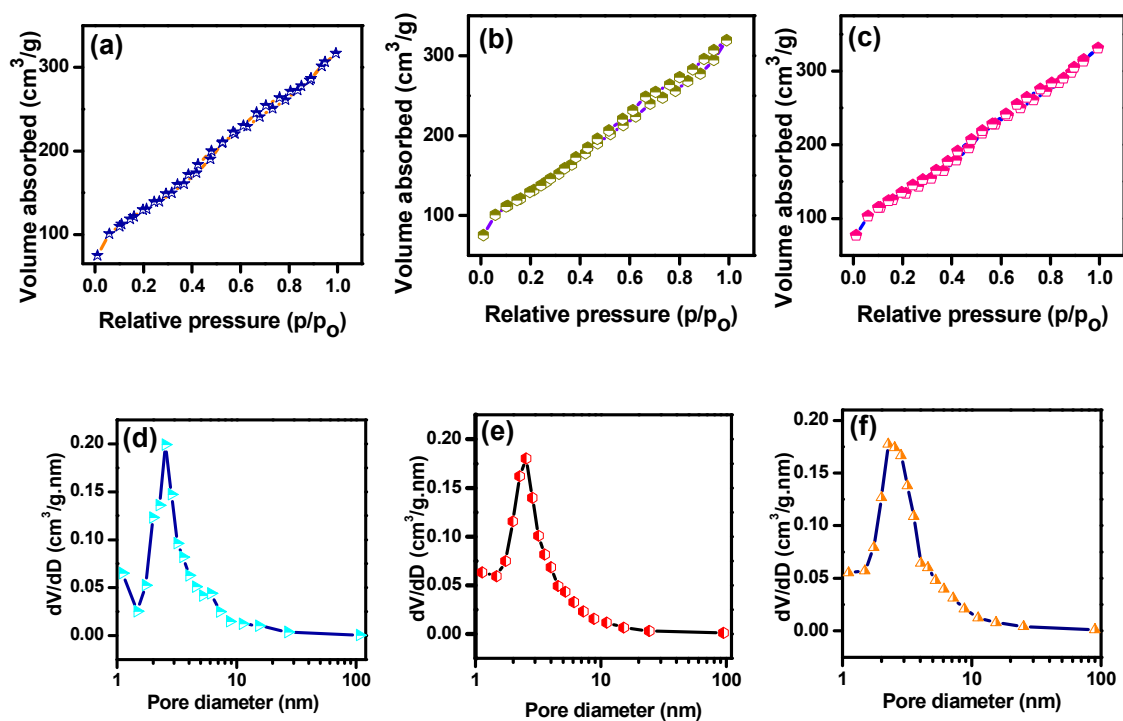

Figure S14: (a, b & c) N_2 adsorption/desorption isotherms and (d, e & f) corresponding BJH pore size distribution plots for Ir@MS-MT with different iridium loading (0.86, 1.33 and 4.72 wt%), respectively.
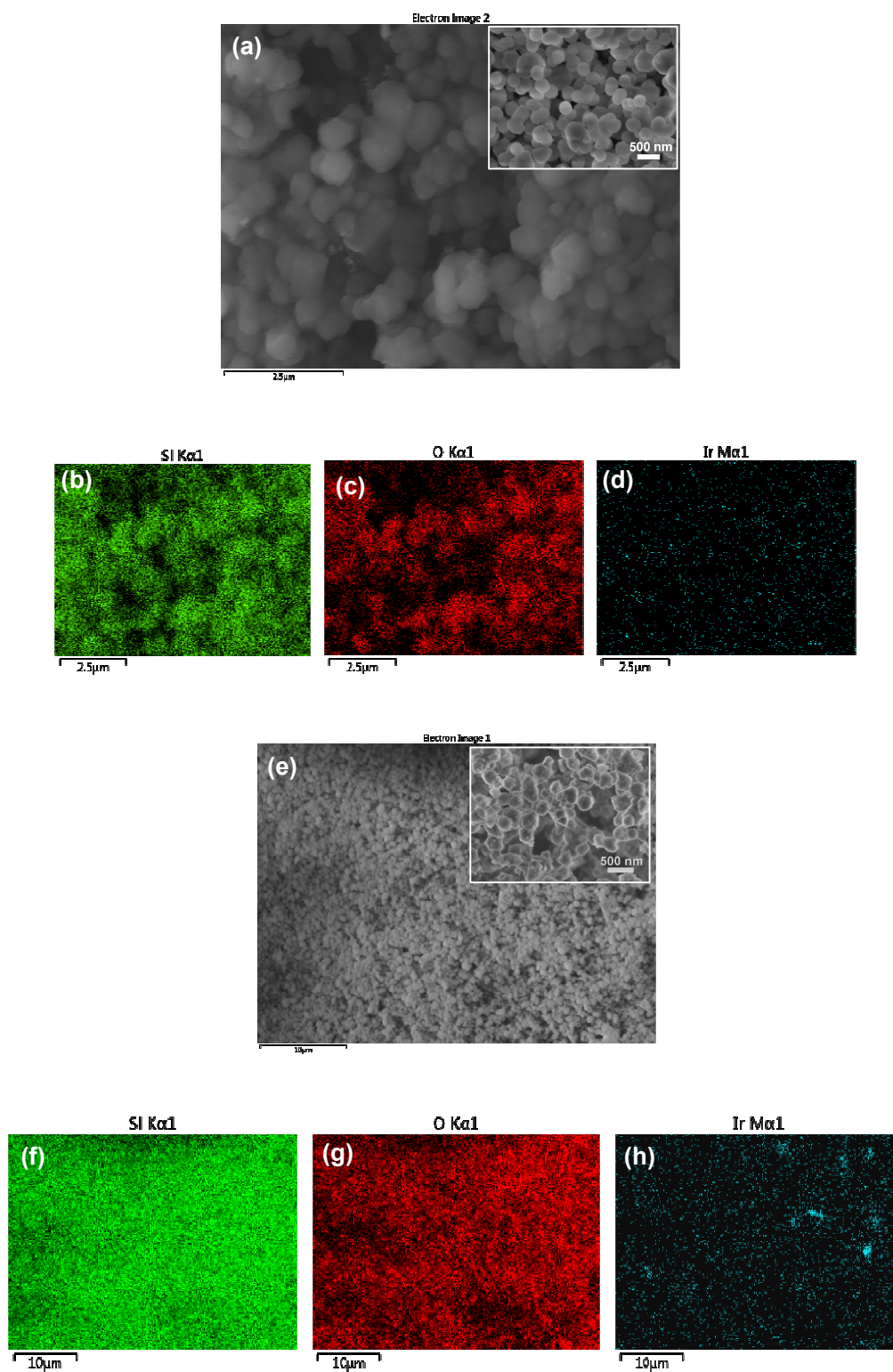
Figure S15: (a & e) FE-SEM images for Ir@MS-MT with different iridium loading (0.86 and 4.72 wt%), respectively (inset: FE-SEM images at higher magnification); (b & f), (c & g), (d & h) corresponding EDX mapping for the elements Si, O and Ir, respectively.
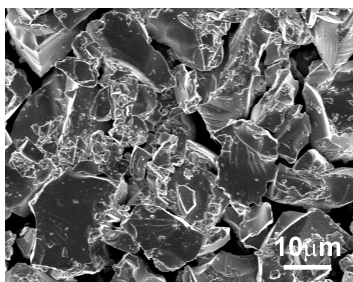
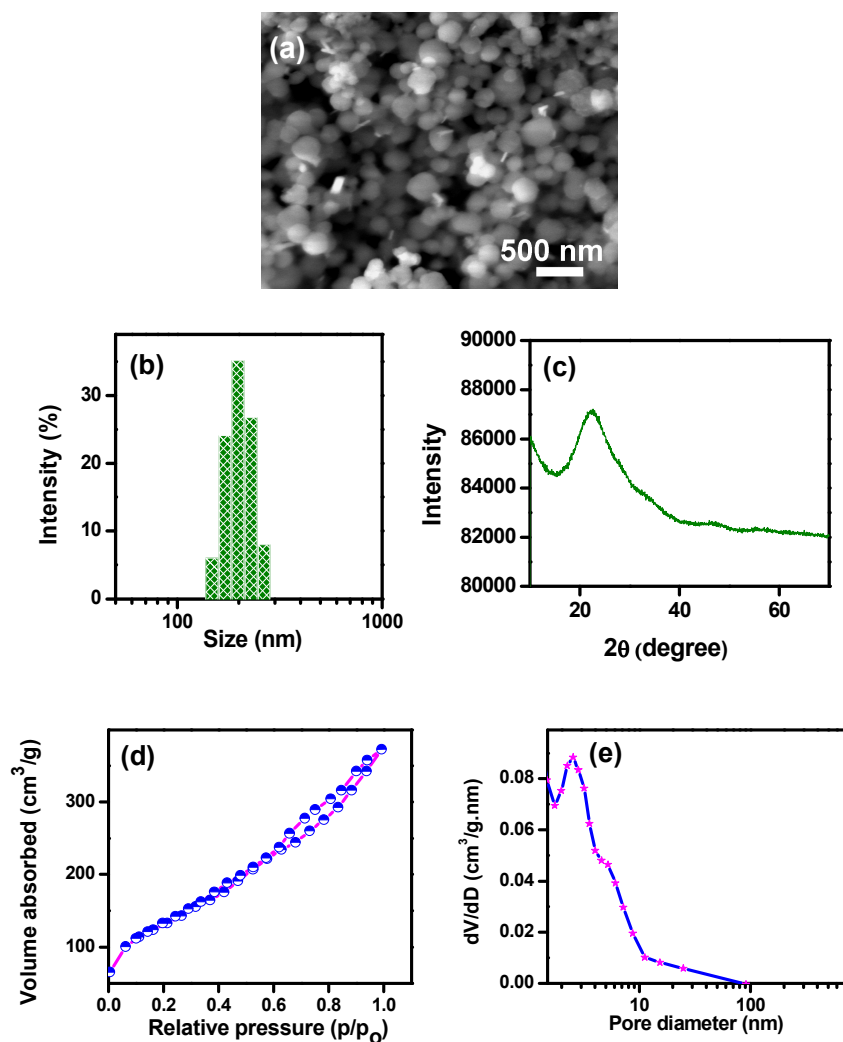Figure S16: FE-SEM image of iridium precursor treated at 573 K for 5 hr.

Figure S17: (a) FE-SEM image, (b) DLS Hydrodynamic particle size distribution, (c) XRD pattern, (d) N_2 adsorption/desorption isotherms and (e) BJH pore size distribution plot for the used Ir@MS-MT sample obtained after fifth cycle of the water oxidation reaction.
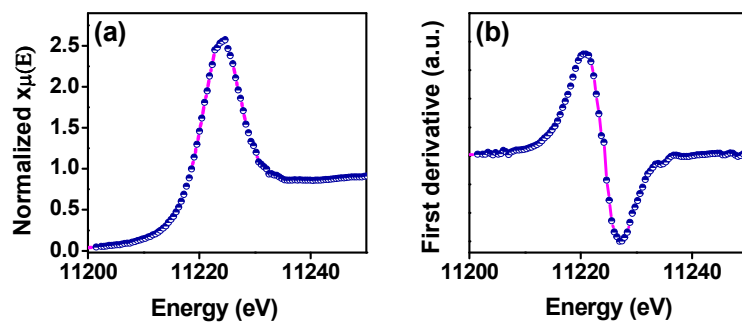
Figure S18: (a) Ir L$_{III}$-edge XANES spectrum, (b) its first derivative for the used Ir@MS-MT after fifth cycle of water oxidation reaction. The LC-XANES fitting showed the composition of Ir oxidation states as Ir(III) (~8%) and Ir(IV) (~92%).

Table S1: Textural properties of MS, MS-PAH and different WOC

Sample		BET surface area (m^2/g)	Average BJH pore size (nm)	Pore Volume (cm^3/g)
MS		980	2.85	0.77
MS-PAH		479	2.84	0.50
Ir@MS-RT		454	2.88	0.49
Ir@MS-MT	0.86 wt% Ir	447	2.75	0.51
	1.33 wt% Ir	459	2.78	0.51
	3.66 wt% Ir	479	2.80	0.52
	4.72 wt% Ir	461	2.50	0.54
Ir@MS-MT used		463	2.81	0.62
Ir@MS-HT		509	2.55	0.61

Table S2: Oxidation states of iridium in WOC as derived from LC fitting of XANES spectra

Sample	Oxidation states of Ir
Ir@MS-RT	Ir(III)
Ir@MS-MT	Ir(III) (~34%) & Ir(IV) (~66%) [a]
Ir@MS-HT	Ir(IV)
IrCl$_3$	Ir(III)
IrO$_2$	Ir(IV)

[a]Values in bracket shows % of respective oxidation states of iridium present in WOC as determined with reference to the standard samples

Table S3: Ir@MS-MT catalysts with different iridium loading and their acticvty in water oxidation reaction. [a]

Catalyst	wt% of Ir	[Ir] µmol[b]	[CAN]/[Ir]	O$_2$ yield (%)	TON[c]
Ir@MS-MT	0.86	0.754	530.5	65	86
	1.33	0.762	524.9	60	78
	3.66	0.759	527.0	77	101
	4.72	0.760	526.3	33	43

[a]400 µmol CAN, pH 1, RT. [b]based on iridium loading on the catalyst as obtained from ICP-OES analysis. [c]TON = moles of O$_2$ evolved/ moles of iridium used.

REFERENCES:

(1)   Poulsen, I. A.; Garner, C. S. *J. Am. Chem. Soc.* **1962**, *84,* 2032.

(2)   Music´, S.; Popovic´, S.; Maljkovic´, M.; Skoko, Zˇ.; Furic´, K.; Gajovic, A. *Mater. Lett.* **2003,** *57,* 4509.

(3)   Hong, D.; Murakami, M.; Yamada, Y.; Fukuzumi, S. *Energy Environ. Sci.* **2012,** *5,* 5708.